



Overview of observations from the RADAGAST experiment in Niamey, Niger: Meteorology and thermodynamic variables

A. Slingo,¹ N. A. Bharmal,¹ G. J. Robinson,¹ J. J. Settle,¹ R. P. Allan,¹ H. E. White,¹ P. J. Lamb,² M. Issa Lélé,² D. D. Turner,³ S. McFarlane,⁴ E. Kassianov,⁴ J. Barnard,⁴ C. Flynn,⁴ and M. Miller^{5,6}

Received 2 February 2008; revised 13 May 2008; accepted 23 June 2008; published 17 October 2008.

[1] An overview is presented of the meteorological and thermodynamic data obtained during the Radiative Atmospheric Divergence using Atmospheric Radiation Measurement (ARM) Mobile Facility, Geostationary Earth Radiation Budget (GERB) data, and African Monsoon Multidisciplinary Analysis (AMMA) stations (RADAGAST) experiment in Niamey, Niger, in 2006. RADAGAST combined data from the ARM Program Mobile Facility (AMF) at Niamey airport with broadband satellite data from the GERB instrument on Meteosat-8. The experiment was conducted in collaboration with the AMMA project. The focus in this paper is on the variations through the year of key surface and atmospheric variables. The seasonal advance and retreat of the Intertropical Front and the seasonal changes in near-surface variables and precipitation in 2006 are discussed and contrasted with the behavior in 2005 and with long-term averages. Observations from the AMF at Niamey airport are used to document the evolution of near-surface variables and of the atmosphere above the site. There are large seasonal changes in these variables, from the arid and dusty conditions typical of the dry season to the much moister and more cloudy wet season accompanying the arrival and intensification of the West African monsoon. Back trajectories show the origin of the air sampled at Niamey and profiles for selected case studies from rawinsondes and from a micropulse lidar at the AMF site reveal details of typical atmospheric structures. Radiative fluxes and divergences are discussed in the second part of this overview, and the subsequent papers in this special section explore other aspects of the measurements and of the associated modeling.

Citation: Slingo, A., et al. (2008), Overview of observations from the RADAGAST experiment in Niamey, Niger: Meteorology and thermodynamic variables, *J. Geophys. Res.*, 113, D00E01, doi:10.1029/2008JD009909.

1. Introduction

[2] Field studies play a important role in providing new data for studying atmospheric processes and for evaluating and improving numerical models. Given the fundamental role of atmospheric radiation in the climate system and of changes in the radiation balance in forcing climate change, observations of radiative fluxes are particularly important. Uncertainties in the radiative properties of clouds continue to motivate airborne campaigns [e.g., Ackerman *et al.*, 2003]. The growing appreciation of the role of aerosols in influencing the radiation budget and climate change, either

directly or indirectly through their impact on cloud properties, is another driver for both airborne studies [Haywood *et al.*, 2003] and for large-scale experiments such as the Indian Ocean Experiment (INDOEX [Ramanathan *et al.*, 2001]). There is thus a continuing need for new observations that can be used to test our understanding of radiative processes and the expression of this understanding in numerical models. These observations should cover the entire range of conditions experienced on the planet. This was a major driver for the Radiative Atmospheric Divergence using Atmospheric Radiation Measurement (ARM) Mobile Facility, Geostationary Earth Radiation Budget (GERB) data, and African Monsoon Multidisciplinary Analysis (AMMA) stations (RADAGAST) experiment, which took place in Niamey, Niger, in 2006. One of the unusual aspects of this experiment was its length; observations were obtained from late 2005 through to the beginning of 2007, providing a record that samples the entire range of conditions through both the dry and wet seasons in 2006.

[3] RADAGAST coordinated surface and remote sensing measurements made by the U.S. Department of Energy ARM Program Mobile Facility (AMF) situated in Niamey (13° 29'N, 2° 10'E) and by the GERB broadband radiometer

¹Environmental Systems Science Centre, University of Reading, Reading, UK.

²CIMMS, University of Oklahoma, Norman, Oklahoma, USA.

³Space Science and Engineering Center, University of Wisconsin-Madison, Madison, Wisconsin, USA.

⁴Pacific Northwest National Laboratory, Richland, Washington, USA.

⁵Brookhaven National Laboratory, Upton, New York, USA.

⁶Now at Environmental Sciences Department, Rutgers University, New Brunswick, New Jersey, USA.

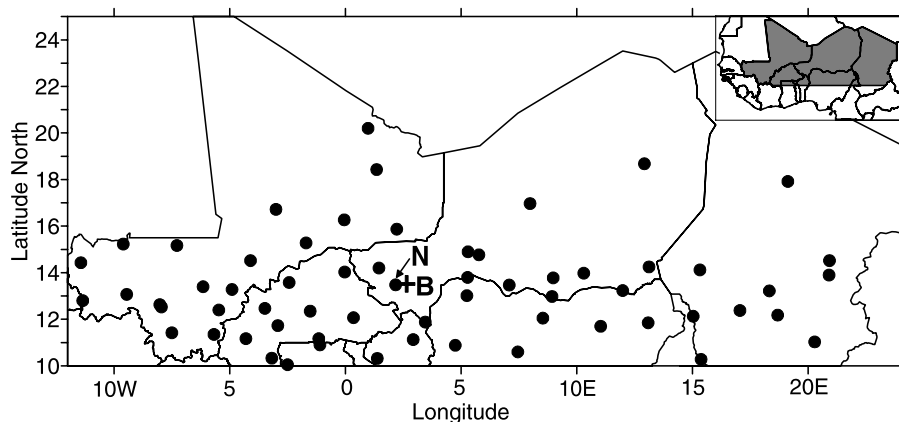


Figure 1. Location of primary (Niamey, N) and ancillary (Banizoumbou, B, cross) observing platforms of the ARM Mobile Facility during 2006 and the stations (including Niamey) from which long-term standard meteorological observations were analyzed to produce Figure 2 (dots).

and multichannel Spinning Enhanced Visible and Infrared Imager (SEVIRI) on the Meteosat-8 operational geostationary satellite (stationed above 0° longitude). The combination of an extended series of broadband measurements both at the surface and from space, backed up by a wide range of passive and active instrumentation, is unique. *Miller and Slingo* [2007] describe the background to RADAGAST and provide details of the instruments deployed at the AMF. Meteosat-8 was the first weather satellite of the Meteosat Second Generation (MSG) series, operated by EUMETSAT. *Schmetz et al.* [2002] provide an introduction to MSG and describe the SEVIRI imager. The GERB radiometer is described by *Harries et al.* [2005].

[4] RADAGAST was timed to coincide with the special observing periods of AMMA, a large international program to study and to improve our understanding of the West African monsoon [*Redelsperger et al.*, 2006]. The measurements complemented those from several other projects within or related to AMMA, in particular the Dust and Biomass Experiment, DABEX [*Haywood et al.*, 2008] in January 2006. Although administered separately, these projects and experiments interacted closely on a daily basis and have shared data in the subsequent analysis of the results. AMMA thus provided an excellent opportunity to foster links between programmes and communities that might otherwise not have interacted with each other.

[5] One important objective of RADAGAST is to derive estimates of the radiative divergence across the atmosphere [e.g., *Slingo et al.*, 2006], but the data also allow many other problems to be studied, beyond those in atmospheric radiation. In particular, the data provide a coherent picture of the seasonal variation of meteorological and associated variables in this sensitive and important climatic region.

[6] This first overview paper discusses the meteorological and thermodynamic observations obtained during the experiment and places them in the context of the long-term average annual cycle at Niamey. In the companion paper, the focus is on the radiative fluxes and divergences and on the factors that control them (A. Slingo et al., Overview of observations from the RADAGAST experiment in Niamey, Niger: 2. Radiative fluxes and divergences, submitted to *Journal of Geophysical Research*, 2008, hereinafter referred

to as Part 2). The subsequent papers in this special section provide detail on further specific studies that have been carried out with the data.

[7] The following section reviews the sources of data and summarizes the processing that was carried out. Section 3 documents the seasonal advance and retreat of the Inter-tropical Front (ITF) and of the associated conditions at Niamey and in the wider region. It also reviews the AMF observations of meteorological and thermodynamic variables at the surface. Section 4 presents observations of the atmospheric structure above the main site. A discussion and review of the results is given in section 5.

2. Data and Processing

[8] The main AMF facility at the Niamey airport site (Figure 1) began making limited observations in November 2005, but routine operations started at the beginning of 2006. The micropulse lidar (MPL) became operational on 27 December 2005, radiosonde ascents started on 7 January 2006 and the cloud radar commenced observations on 16 March 2006. Most instruments at the airport site in Niamey operated continuously until 7 January 2007, although the cloud radar ceased operations on 24 December 2006. The more limited measurements from the ancillary site at Banizoumbou, about 50 km east of Niamey (Figure 1), cover the period from 26 December 2005 to 8 December 2006. The AMF results shown here are for the calendar year 2006, which covers the period when most of the instruments at both sites were operating and provides a continuous data record that spans a complete seasonal cycle. Details of all the instruments are provided by *Miller and Slingo* [2007].

[9] To set the AMF results in context, they are preceded by a brief documentation of the long-term average annual climate cycle at Niamey, based on standard meteorological observations. The data were obtained from the Directions de la Météorologie Nationale (National Weather Services) of Niger and surrounding countries. Data for 2006 are compared with this background information in the following section.

[10] Data from Meteosat-8 are not presented in this paper, but a cloud mask derived from the data is used in Part 2 in

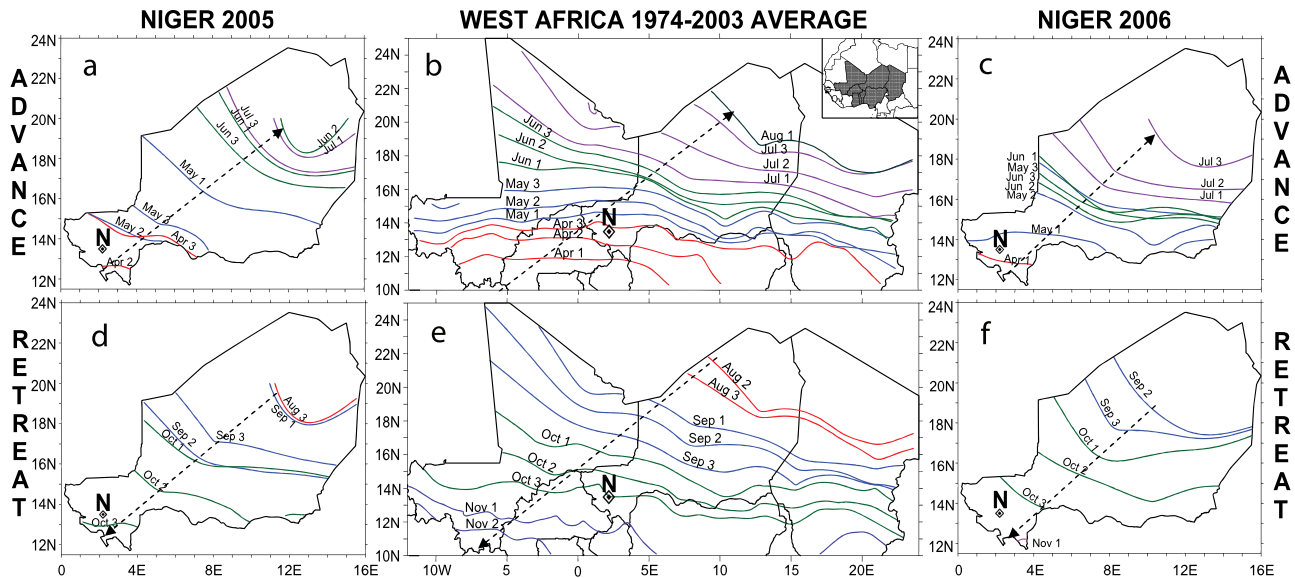


Figure 2. ITF (a–c) advance and (d–f) retreat across West Africa, demarcated using 15°C dew point isotherm (see section 3.1) derived from meteorological observations for stations located by dots in Figure 1. Figures 2b and 2e show the long-term average for 1974–2003 for most of West Africa, and Figures 2c and 2f (Figures 2a and 2d) are for Niger only for the AMF deployment year of 2006 (comparison year of 2005). ITF locations given are averages for 10-day periods in each month (dekads, labeled 1, 2, and 3), with lines for each month having the same color. Broken arrows indicate directions of ITF advance and retreat. N locates Niamey. The pattern for Niger 2006 advance does not contain ITF locations for the second and third dekads of April, because the ITF retreated south of 12°N during that time. During the July–August 2005 and August–September 2006 dekads for which the ITF is not delineated, it was north of the northernmost station in Figure 1.

the analysis of the radiative fluxes (Slingo et al., submitted manuscript, 2008). The following discussion is included here for completeness, since in carrying out the experiment both the AMF and satellite data were examined on a daily basis, in order to monitor conditions and to identify case studies for further detailed examination.

[11] Meteosat-8 was launched in August 2002 and ran continuously until Meteosat-9 took over as the operational satellite in April 2007. This changeover was much later than planned by EUMETSAT, because of anomalies with the SEVIRI instrument on Meteosat-9 that took a long time to resolve. This delay actually had a positive impact on RADAGAST, because it meant that Meteosat-8 operated throughout the experiment, so the need to merge data from the two satellites was avoided. Apart from very short periods, data from the SEVIRI instrument are available continuously throughout 2006. GERB data are also available for most of the year (see Part 2 for further discussion).

[12] The satellite data were processed at the Environmental Systems Science Centre (ESSC) for a large study area (approximately 5°S to 30°N and 30°W to 30°E). SEVIRI level 1.5 data over this region were extracted by the EUMETSAT Archive Operations Division and sent by ftp to a dedicated server at ESSC in near real-time (latency about 30 min). The processing of the GERB data is described in Part 2. The satellite data were processed to display images on the project website of all the SEVIRI bands and of the dust and water vapor products, plus GERB shortwave and longwave radiances and fluxes, at the full time and space resolution. To complement the satellite

images, selected AMF quicklook products were retrieved from the ARM server and also displayed (latency about 1 h). Animation of the satellite and AMF products on a daily basis enabled interesting events to be identified in a timely manner and a log of the whole year was maintained for future reference. The Web site was also used by several other groups within AMMA.

3. Analysis of Results: Surface Variables

[13] The meteorological conditions at Niamey and the surrounding region in 2006 are reviewed below and compared with the climatology of the region. This is followed by an analysis of the main surface meteorological variables measured at the airport site.

3.1. West African Intertropical Front and Rainfall

[14] Standard meteorological observations from Niamey and elsewhere in West Africa are used here to provide background information on the atmospheric behavior over West Africa that is most pertinent for the AMF deployment in Niamey (Figure 1). The analyses have 10-day (dekadal, Figures 2 and 3) and seasonal (Figure 4) mean time scales.

[15] The measurements made at and above Niamey throughout 2006 by the AMF's suite of vertically pointing instruments [Miller and Slingo, 2007] reflect the annual cycle of the West African monsoon system. Fundamental to this monsoon annual cycle is the northward advance and southward retreat of the surface Intertropical Front (ITF). During the monsoon season from June–September, the ITF

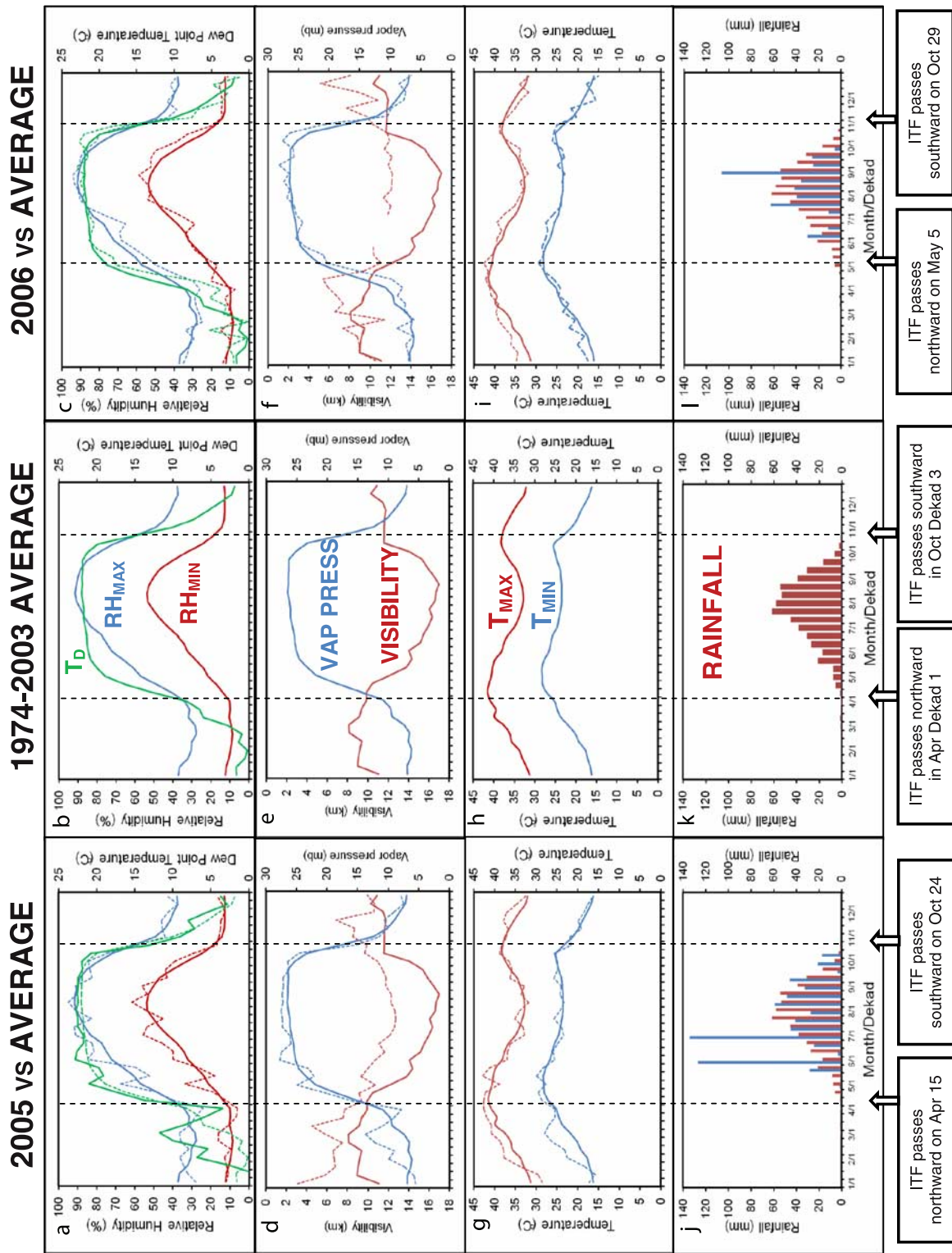


Figure 3

separates the warm, moist, southwest monsoon flow from the tropical Atlantic and the much hotter, drier, dusty, northeasterly Harmattan air from the Sahara. The interface between the two air masses slopes upward toward the south through the lowest 300 hPa of the atmosphere at average inclinations that vary seasonally in the 1:100 to 1:400 range, with the monsoon flow undercutting the Harmattan air in a wedge-like manner [Hastenrath and Lamb, 1977; Hastenrath, 1991, pp. 166–174]. During the dry season, the zone of maximum insolation and the ITF move well to the south of Niamey (as far as the Gulf of Guinea coast), when the cooler, dusty, northeasterly Harmattan flow undercuts the warmer tropical air to the south [e.g., Haywood *et al.*, 2008]. Accordingly, the total column water vapor (near-surface dust load) above Niamey maximizes when the ITF is far north (south) of that location, and vice versa.

[16] Using a traditional ITF demarcation of sustained 15°C surface dew point temperature [Eldridge, 1957; Ilesanmi, 1971; Lélé, 2007], Figures 2b and 2e document the long-term (1974–2003) average annual cycle of the surface ITF position across most of West Africa between 10° and 25°N. The ITF's average northward advance through this zone occurs slowly between the first dekad of April and the first dekad in August, with the subsequent average southward ITF retreat between the second dekad of August and the second dekad of November being almost 50 percent more rapid. Northward from Niamey, the ITF has an increasing WNW-ESE orientation. Monsoon air thus typically resides over Niamey between the first dekad of April and the last dekad of October (approaching seven months), with the depth of the layer increasing to a maximum in late July and early to mid-August and then decreasing. These conditions characterize other West African locations at approximately the same latitude as Niamey.

[17] Figures 3b, 3e, 3h, and 3k document the average association of the above ITF annual cycle with atmospheric variables at Niamey that are key to interpreting the AMF measurements there. Most fundamental is the seasonal rainfall variation shown in Figure 3k. The zone of maximum rainfall occurs approximately 300 km south of the ITF, and advances northward/retreats southward in tandem with the ITF, because the convective systems involved [Bell and Lamb, 2006] require the support of a well-developed moist monsoon layer. As a result, Niamey's monsoon rainfall usually commences very modestly in April-May, then increases markedly and progressively to a late July-entire August maximum, after which it declines much more

abruptly through September and October. The December–February period is always rainless, and rain seldom occurs in November or March. This slow development and much faster cessation of monsoon rain at Niamey are fully consistent with the relative rates of ITF advance and retreat shown in Figure 2. The same seasonal pattern prevails across the entire Soudano-Sahel zone of North Africa, from Senegal in the west to Ethiopia in the east [Segele and Lamb, 2005; Bell and Lamb, 2006; Lélé, 2007].

[18] Associated with the mean annual cycles of the ITF and Niamey monsoon rainfall are distinctive variations of other atmospheric parameters that influenced the AMF measurements in Niamey (Figures 3b, 3e, and 3h). The basic moisture parameters (dew point temperature, vapor pressure) not only increase strongly during the March-May period straddling the northward ITF passage through Niamey, but thereafter continue to increase modestly until late September. Pronounced dew point and vapor pressure decreases occur during October-December. In contrast, the average annual cycle of relative humidity is bell shaped and near symmetrical about a mid-August maximum, with slower rates of monsoonal increase (especially) and decrease than for dew point and vapor pressure. This relative humidity pattern results from its partial control by air temperature, most notably the premonsoon (mid-April to early May) and postmonsoon (mid-October) temperature maxima and the midmonsoon (mid-August) temperature minimum. The first (and primary) temperature maximum occurs at the end of the dry season, when the land surface is driest and incoming solar radiation is near maximum at 13°N. The latter circumstance and postmonsoon reduced cloudiness contribute to the secondary temperature maximum in October. The intervening temperature minimum centered on mid-August results from reduced incoming solar radiation and the increasing cloud cover, surface wetness, and evapotranspirative cooling that accompany the progressive increase of monsoon rainfall from May through August.

[19] Other striking aspects of Figures 3b, 3e, 3h, and 3k concern the mean annual cycle of visibility. Both dust and smoke aerosol play an important role in the surface radiation balance during the dry season [Milton *et al.*, 2008]. However, dust is the predominant aerosol at low altitudes and therefore is the major influence on surface observations of visibility. Accordingly, visibility can be used as a proxy for near-surface dust (A. Ben Mohamed *et al.*, Atmospheric dust in the West African Sahel and ocean-atmosphere climate variations on seasonal, interannual and multi-decadal time-scales, submitted to *International Journal of*

Figure 3. (a–l) Annual cycles of key atmospheric variables at Niamey, given by mean values for 10-day (dekad) periods. Figures 3b, 3e, 3h, and 3k give long-term averages for 1974–2003 for most of West Africa, and broken lines and blue bars in Figures 3c, 3f, 3i, and 3l (Figures 3a, 3d, 3g, and 3j) relate annual cycles for AMF deployment year of 2006 (comparison year of 2005) with their long-term average counterparts in Figures 3b, 3e, 3h, and 3k. T is surface air temperature, and RH is surface relative humidity, with subscripted MAX and MIN indicating daily maximum and minimum values, respectively. T_D is surface dew point temperature, and VAP PRESS is surface vapor pressure, both at the time of daily minimum surface air temperature. Visibility (averages of hourly values) is used as a proxy for near-surface atmospheric dust loading, hence its inverted ordinate. The cause of the reduced visibility values for 2005–2006 relative to the 1974–2003 average is not yet clear; possibilities include changed observing practices and increased aerosols from burning and land degradation (A. Ben Mohamed, personal communication, 2008). However, the annual visibility cycles for 2005–2006 are considered reliable and so are compared in the text. Broken vertical lines indicate dates of northward and southward ITF passage through Niamey (see also Figure 2).

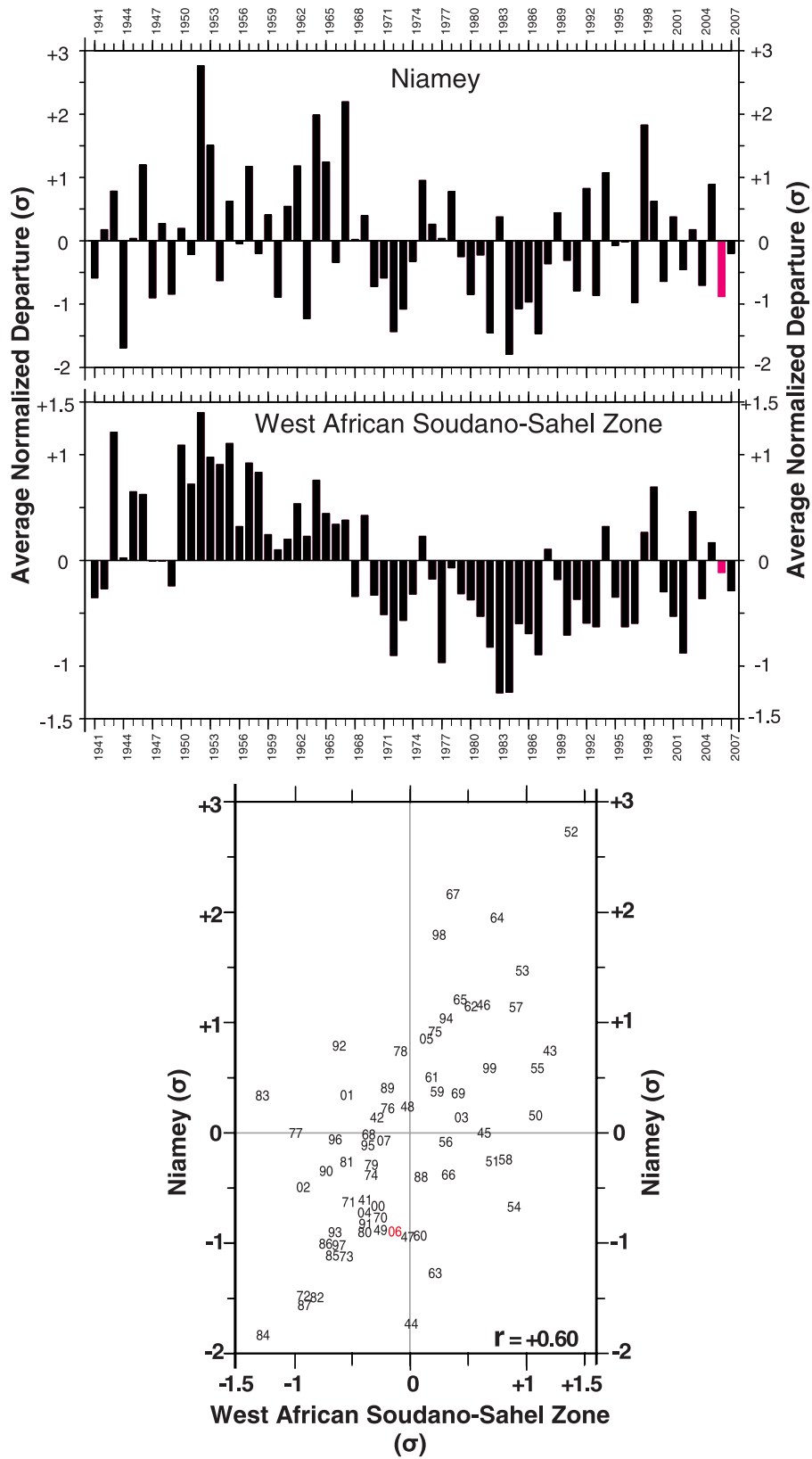


Figure 4. Normalized April–October rainfall departure indices (σ) for (top) Niamey and (middle) the entire West African Soudano-Sahel Zone for 1941–2007 and (bottom) their relationship (where the numbers give the last two digits of the years). Values for 2006 are in red. The West African index is averaged across 20 stations between 11 and 18°N and west of 10°E located in the work by *Lamb* [1978, Figure 1], including Niamey. The normalization procedure used station means and standard deviations for 1941–2000. In Figure 4 (bottom), r gives the linear correlation coefficient.

Climatology, 2008). The visibility scale in Figure 3 is inverted to emphasize that high visibility corresponds to low dust, and vice versa. Visibility is lowest (dust greatest) in late February to early March, near the end of the dry season, after which visibility increases (dust decreases) strongly to be almost doubled by late August. As with most other parameters in Figure 3, September–October is a period of pronounced change (decrease) for visibility (increased dust), after which the visibility decrease is more modest through the late February to early March minimum. Also evident in Figure 3 is a very strong positive relationship between visibility and vapor pressure. The linear correlation between the long-term dekadal means of these parameters in Figure 3e is +0.90 (significant at 0.001% level according to a two-tailed t test), and the correlation between the contributing individual dekadal averages is +0.66 (0.001% significance). This strong inverse relation between the atmospheric presence of Harmattan dust and monsoon water vapor is a dominant feature of Niamey's annual climate cycle.

[20] Figure 4 shows that the total monsoon seasonal rainfall at Niamey is quite representative of the entire West African Soudano-Sahel zone within which it resides, on both the interannual and multidecadal time scales. Relative to the period since 1941, West African Soudano-Sahel monsoon rainfall was deficient during the AMF deployment in 2006 (Figure 4). This was especially characteristic of the AMF site in Niamey (-0.88σ) and of several other AMMA rain gauges within 45 km (-1.03σ to -1.78σ , using the 1941–2000 mean and standard deviation for Niamey), but less so for the AMF ancillary site at Banizoumbou (-0.32σ , using Niamey standardization statistics) and the West African Soudano-Sahel zone as a whole (-0.29σ). Averaged over 29 AMMA rain gauges within 95 km of Niamey, the 2006 rainfall departure (-0.27σ , using Niamey standardization statistics) was very close to the zone-wide mean. Figure 4 also shows that rainfall in the immediately preceding monsoon season (2005) was more abundant at (especially) the Niamey AMF site ($+0.89\sigma$) and for the entire West African Soudano-Sahel zone ($+0.17\sigma$).

[21] Figures 2c, 2f, 3c, 3f, 3i, and 3l show the ITF advance and retreat across Niger during the AMF deployment year (2006), and the annual cycle response at the Niamey AMF site of atmospheric variables that are key for interpreting the AMF measurements there. For comparative purposes, Figures 2a, 2d, 3a, 3d, 3g, and 3j provide the same documentation for the much wetter 2005. During the 2006 AMF deployment, the monsoon was anomalously dry at Niamey in several respects. The ITF's northward passage through Niamey was delayed until about a month after the 1974–2003 average date, whereas it was only a few days after that average in 2005 (Figures 2 and 3). Consistent with these ITF differences, the early season (May–July) rainfall at the Niamey AMF site was only 60% of the 1941–2000 average during 2006, whereas it was 157% in 2005 (Figure 3). After near-average peak season (total August) rainfall in 2006, the end-of-season (September–October) rainfall total was even more deficient (53% of the 1941–2000 average) than the early season amount. In contrast, despite below average August rainfall at the Niamey AMF site in 2005, the August–October total for that year still exceeded that during the 2006 AMF deployment.

[22] The delayed northward ITF passage through Niamey in 2006 was also manifest there in a retarded initiation of the plateau-like monsoon maxima of dew point and vapor pressure and the associated visibility increase, in later (early May) temperature maxima and slower than average temperature declines thereafter, and in a concomitant suppression in relative humidity increase (Figures 3c, 3f, 3i, and 3l). The earlier northward ITF passage in the wetter 2005 was associated with the opposite dew point, vapor pressure, visibility, temperature, and relative humidity anomalies (Figures 3a, 3d, 3g, and 3j). Anomalous end-of-season characteristics for 2006 in Niamey include pronounced secondary temperature maxima in early to mid-October (consistent with the seasonal dryness), a slightly delayed southward ITF passage, and an associated extension through October of near annual maximum visibility and the plateaus of maximum dew point and vapor pressure. None of these anomalies characterized the wetter 2005. Interestingly, the Niamey AMF site received no rain in October 2006 despite the persistence of surface monsoon moisture there throughout that month. While rain also was absent from Niamey in October 2005, in that case the surface monsoon moisture had retreated to the south by midmonth.

3.2. Surface Variables at the Main Niamey Airport Site

[23] The surface variables measured at the Niamey airport site in 2006 are presented here with a temporal resolution of one day, which builds on the climatological comparisons presented above and provides further detail for the results shown later and in Part 2. Daily averaging also prevents the substantial diurnal and higher-frequency variability from obscuring the slower synoptic to seasonal time scale variations that are the main focus of this paper.

[24] The evolution of the screen-level temperature, dew point temperature and relative humidity is shown in Figure 5. Temperatures were high throughout the year, with the maximum at the end of the dry season and a lesser maximum at the end of the wet season. At the start of the year, humidities were typical of the dry season, with dew points well below 0°C , except during isolated episodes when relatively moist air was advected over the site (see below). As the dry season progressed, temperatures increased and dew points decreased slightly, so there was a distinct decrease in the relative humidity, with the lowest values occurring just before the onset of the summer monsoon. While it is possible that this decrease is due to the progressive drying of the surface upstream of Niamey following the previous year's wet season, there is large interannual variability in the seasonal progression of humidity, with no clearly reproducible pattern from year-to-year (A. Ben Mohamed, personal communication, 2008).

[25] As discussed earlier, the onset of the rains, marked by the northward passage of the ITF through Niamey (Figures 3c, 3f, 3i, and 3l) and defined as occurring when dew points are consistently higher than 15°C , took place later than usual on 5 May, but this was preceded by a “false onset” in the middle of April. While no significant rainfall was associated with this event, Figure 5 shows that in other respects it marked the arrival of moist air associated with the southwest monsoon, which then retreated and only returned

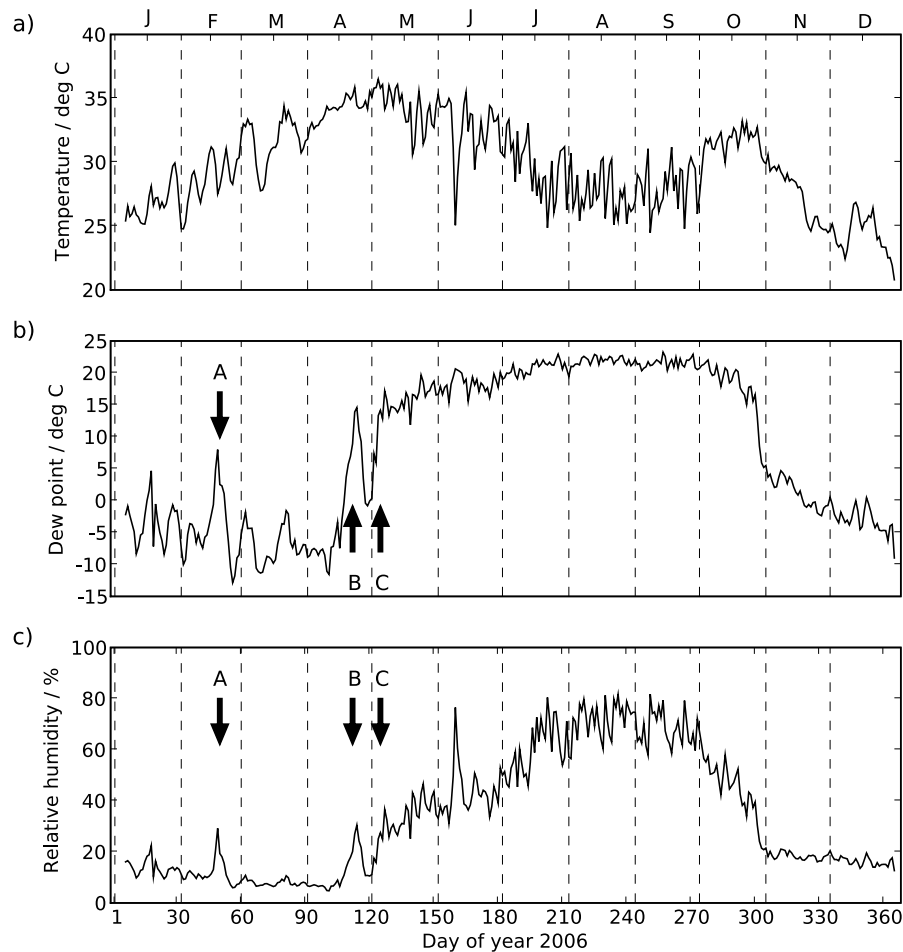


Figure 5. Daily mean (a) screen-level temperature ($^{\circ}\text{C}$), (b) dew point temperature ($^{\circ}\text{C}$), and (c) relative humidity (percent) during 2006 at the Niamey airport AMF site. The abscissa shows the day number in 2006, and the dashed vertical lines denote the boundaries between the calendar months, the first letters of which are indicated at the top of the figure. The arrows indicate the synoptic event from 15 to 22 February (A), the false onset of the wet season in mid-April (B), and the actual onset on 5 May (C). See text for discussion.

on 5 May, much later than the normal onset date (for further discussion see section 3.1).

[26] During the wet season, the temperatures decreased with time, but the dew points increased, the lowest temperatures and highest relative humidities occurring at about the end of August. Temperatures and dew points show pronounced high-frequency temporal variability in the wet season, associated with day-to-day variability in convection. In the dry season, the variability is associated with much slower synoptic-scale variability. The end of the wet season was marked by a precipitous drop in the dew point, with the ITF passing southward through Niamey on 29 October. Thereafter, conditions returned to those typical of the dry season.

[27] Surface winds (Figure 6) show the characteristic shift in direction between the northeasterly Harmattan winds in the dry season to the southwesterly winds of the monsoon, with a slow transition during the false onset. In contrast, as with the other variables, the change is particularly rapid at the end of the wet season. It is also apparent that the humidity variations in the dry season shown in Figure 5

are correlated with changes in wind direction seen in Figure 6, suggesting that the cause is advection of moist air from sources less dry than in the climatological direction.

4. Analysis of Results: Atmospheric Structure

[28] This section presents data on the vertical structure of the atmosphere over Niamey through 2006. In sections 4.1 and 4.2, summaries of the winds, temperatures and humidities from the ARM rawinsondes launched from the airport site are presented. In section 4.3, back trajectories calculated by the HYSPLIT model provide insight into the history and origin of the air over Niamey through the year. In section 4.4, examples of individual sondes and corrected MPL backscatter plots are shown to illustrate particular cases in more detail and to provide background for the following papers.

4.1. Winds

[29] One major resource from the AMF deployment is the archive of rawinsonde ascents through almost the whole of

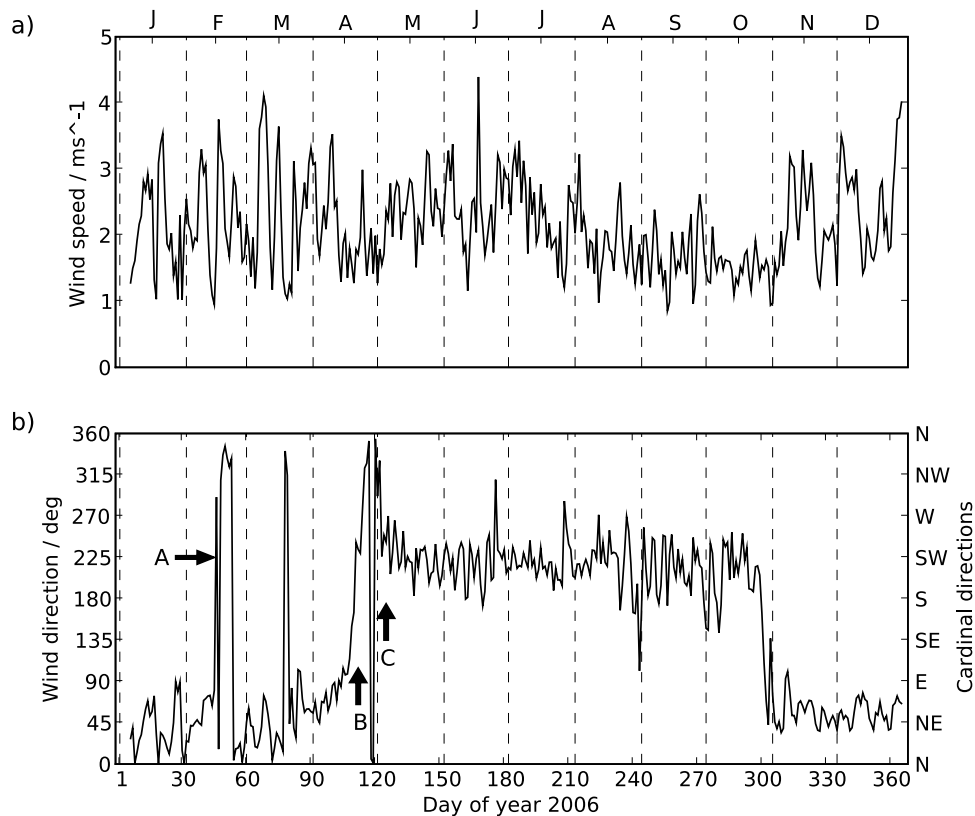


Figure 6. Daily mean (a) surface wind speed (m s^{-1}) and (b) surface wind direction (degrees from north: the cardinal and intercardinal directions are shown on the right), during 2006 at the Niamey airport AMF site. The abscissa shows the day number in 2006, and the dashed vertical lines denote the boundaries between the calendar months, the first letters of which are indicated at the top of the figure. The arrows indicate the synoptic event from 15 to 22 February (A), the false onset of the wet season in mid-April (B), and the actual onset on 5 May (C). See text for discussion.

2006, with an unprecedented frequency for the west African Sahel of four per day. Examination of individual ascents reveals a richness of atmospheric structure, with many distinct layers, even during the wet season. Some examples are shown later. Here, the diurnally averaged wind speed and direction as a function of height are plotted through the year in Figure 7. Several interesting features are apparent and may be compared with the study by *Nicholson and Grist* [2003], who used the NCEP-NCAR reanalysis, and with the ERA-40 reanalysis atlas [*Källberg et al.*, 2005]. At the start and end of the year, the southern flank of the subtropical westerly jet is over Niamey, so that west to southwesterly winds are evident in the mid-to-upper troposphere, with peak winds around 200 hPa. Synoptic events associated with midlatitude disturbances disrupt the flow, in some cases (e.g., from 15 to 22 February) leading to the advection of anomalously moist air over Niamey, while in others leading to the advection of the cold, dry air associated with the major dust storm in early March [*Slingo et al.*, 2006].

[30] From January through May, the subtropical jet weakens and moves toward the summer (northern) hemisphere, which manifests itself on Figure 7 as an elevation of the height of the boundary between westerly and easterly winds [cf. *Nicholson and Grist*, 2003, Figure 3]. During July and August, the upper level westerlies are replaced by the

easterlies associated with the Tropical Easterly Jet (TEJ), visible at around 100 hPa on Figure 7. Lower down, the African Easterly Jet (AEJ) becomes established at about 600 hPa in May and persists until the end of October. Lower still, the southwesterly winds of the shallow monsoon layer may be seen, extending from the surface to around 800 hPa. There is strong shear between the AEJ and the monsoon flow. Many other features on shorter time scales are apparent in Figure 7 and merit further investigation.

4.2. Temperatures and Humidities

[31] The time series of diurnally averaged potential temperature (Figure 8a) and water vapor mass mixing ratio (Figure 8b) show that the structure of the atmosphere below 500 hPa changed significantly through the year. In the dry season up to the middle of March, episodes of relatively cool air can be seen below about 800 hPa, culminating in the major dust storm which peaked on 8 March. This event is dry, but in the earlier events there is no clear correlation between temperature and moisture. Elevated moist layers are apparent, up to about 600 hPa. From mid-March through April, the potential temperature gradient below 700 hPa is weak, indicative of deep well-mixed dry convective layers. The false onset in April is apparent in the moisture field, but the temperature structure only changes with the beginning of the wet season on 5 May, when there is a marked

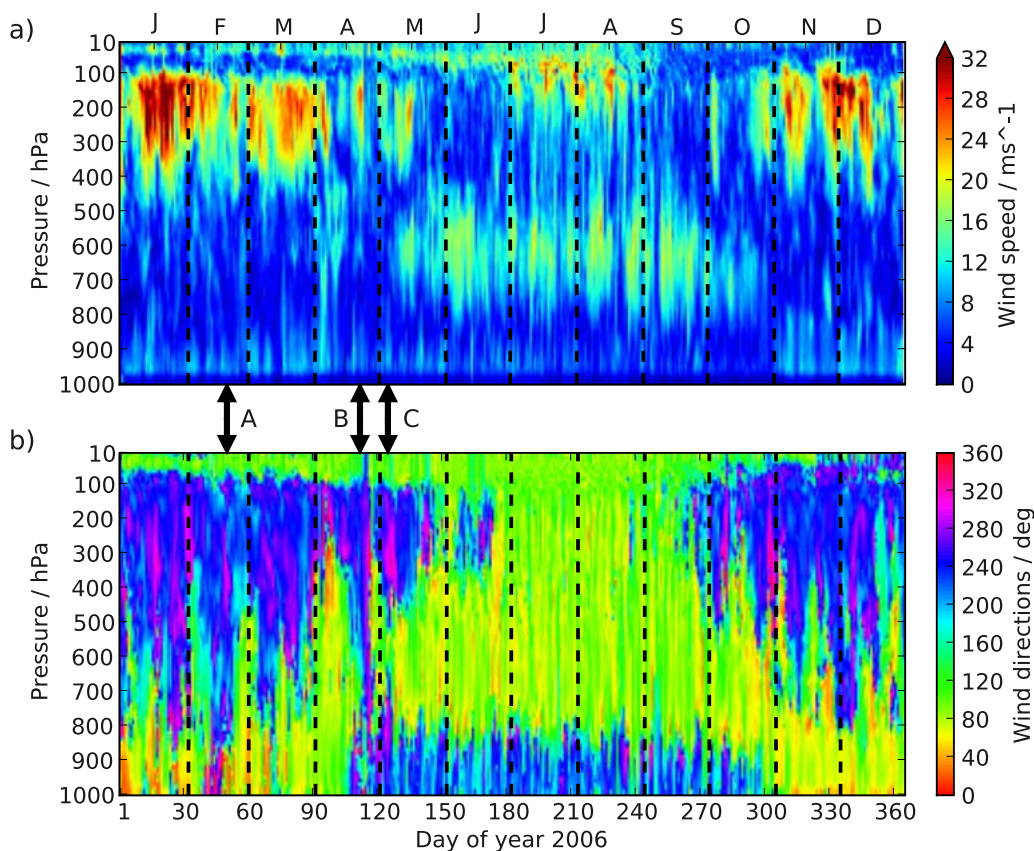


Figure 7. Vertical profiles of daily mean (a) wind speed (m s^{-1}) and (b) wind direction (degrees from north), from AMF sondes launched during 2006 from the Niamey airport site. The abscissa shows the day number in 2006, and the dashed vertical lines denote the boundaries between the calendar months, the first letters of which are indicated at the top of the figure. The arrows indicate the synoptic event from 15 to 22 February (A), the false onset of the wet season in mid-April (B), and the actual onset on 5 May (C). See text for discussion.

reduction in the depth of the near-surface mixed layer as the monsoon air arrives. Thereafter, temperatures below 800 hPa fall and the moisture content rises, in agreement with Figure 5. The near-surface layer becomes more shallow near the end of the wet season, which is marked by a dramatic drop in the boundary layer moisture content as the ITF passes southward. In the subsequent dry season, elevated moist layers return occasionally and the boundary layer structure is similar to that at the beginning of the year, although somewhat colder and drier. Some of these features are shown in more detail in section 4.4, in which individual sonde ascents are presented, together with the corresponding backscatter profiles from the MPL.

[32] Figure 8c shows the column water vapor (CWV) calculated from the sonde data, with the values derived from the microwave radiometer (MWR [see *Miller and Slingo, 2007*]) overplotted in gray. The latter use the improved MWRRET algorithm described by *Turner et al. [2007]*. The agreement between the sonde and MWR estimates of the CWV is extremely good. There is also a close correspondence between the CWV and the dew points shown in Figure 5b, which is expected since the CWV is dominated by humidities near the surface, although there are also some significant differences during the dry season and particularly near the end of the year. At these times, the sondes show

considerable structure in the vertical profile of humidity, so the surface dew point is not such a good guide to the value of the CWV as it is during the monsoon.

[33] One of the motivations for deploying the AMF in Niamey was the large seasonal variation in the CWV [see *Miller and Slingo, 2007, Figure 4*]. Figure 8c shows that this was certainly justified: the observed sonde values range from 3 mm on 11 April to over 60 mm on a few days during the wet season. This large range has a profound impact on the radiative fluxes, as shown in Part 2. The nature of the variability also changes between the relatively slow dry season oscillations associated with the midlatitude synoptic events mentioned earlier, to the high-frequency variability arising from squall lines and individual convective systems in the wet season.

4.3. Back Trajectories

[34] Back trajectories provide valuable information on the origin of the air over the few days prior to its arrival at Niamey, and so aid further the interpretation of the AMF measurements. In particular, the mineral dust composition, as inferred from spectral infrared measurements made at the AMF site, suggests that there is a dependence on the trajectory direction (D. D. Turner, Ground-based infrared retrievals of optical depth, effective radius and composition

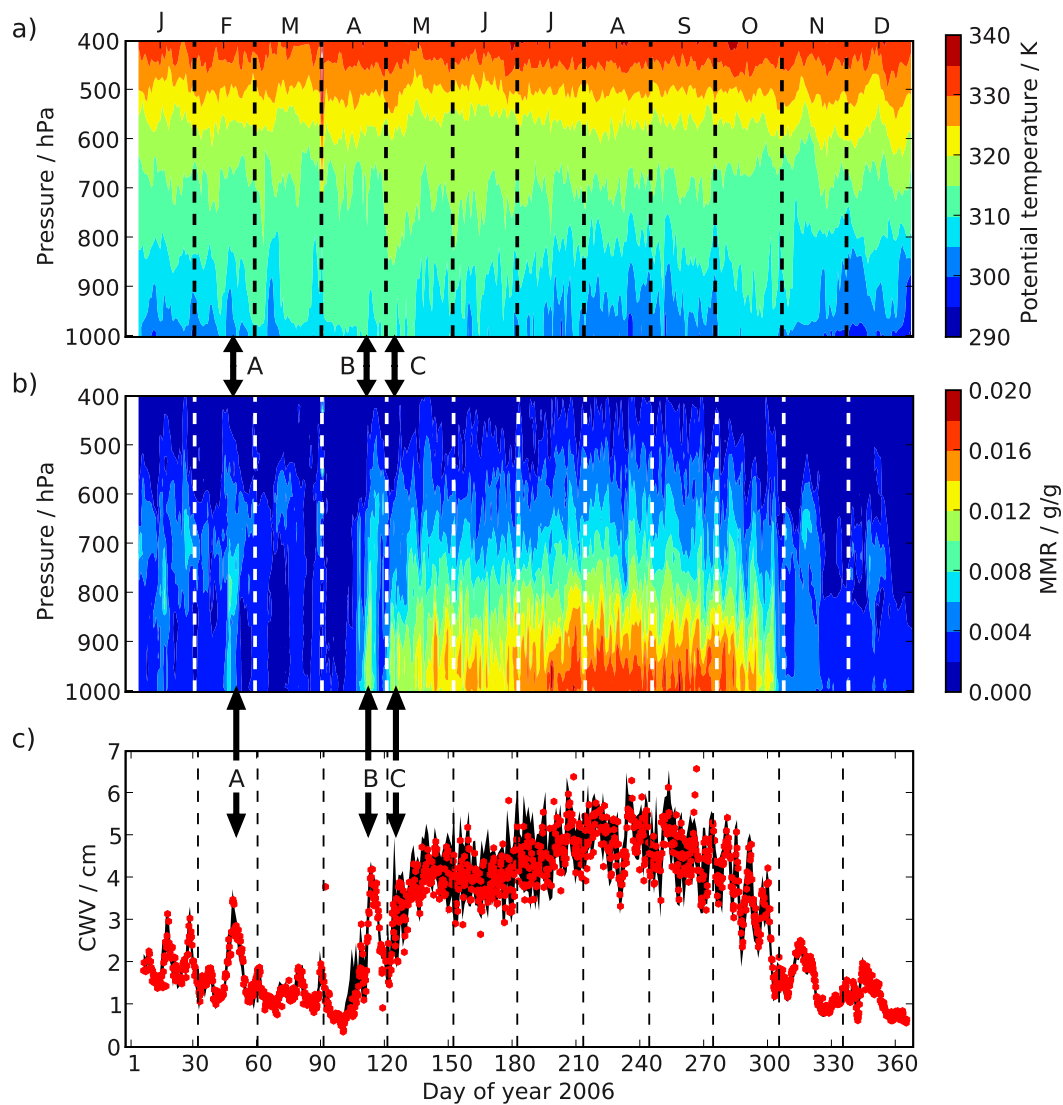


Figure 8. Vertical profiles of daily mean (a) potential temperature (K) and (b) water vapor mass mixing ratio (g/g), from AMF sondes launched during 2006 from the Niamey airport site. (c) Column water vapor (cm) derived from the sondes (red points) and from the microwave radiometer (black background). The abscissa shows the day number in 2006, and the dashed vertical lines denote the boundaries between the calendar months, the first letters of which are indicated at the top of the figure. The arrows indicate the synoptic event from 15 to 22 February (A), the false onset of the wet season in mid-April (B), and the actual onset on 5 May (C). See text for discussion.

of airborne mineral dust above the Sahel, submitted to *Journal of Geophysical Research*, 2008). In this subsection, back trajectories calculated using Version 4 of the HYSPLIT model [Draxler, 2006] are shown. The trajectory calculations used analyses from the National Centers for Environmental Prediction (NCEP) Global Data Assimilation System (GDAS).

[35] Figure 9 shows back trajectories calculated for air arriving at Niamey at heights of 500 m, 1 km, and 4 km at 1200 UTC on each day of 2006. Each trajectory is 72 h long and each line on these plots represents the trajectory arriving at the specified level on 1 day. The plots are split into four seasonal periods: the dry season from the beginning of 2006 up to 14 April, near the end of which there is

Figure 9. Back trajectories over 72 h, calculated from HYSPLIT. Each line shows the trajectory of air arriving at Niamey at 1200 UTC on each day during 2006 at heights of (a–d) 500 m, (e–h) 1000 m, and (i–l) 4000 m. To further document the annual cycle, the trajectories are separated into four periods: 1 January to 14 April (Figures 9a, 9e, and 9i), 15 April to 3 July (Figures 9b, 9f, and 9j), 4 July to 28 October (Figures 9c, 9g, and 9k), and 29 October to 31 December (Figures 9d, 9h, and 9l). The location of Niamey is marked by the open circle in each panel.

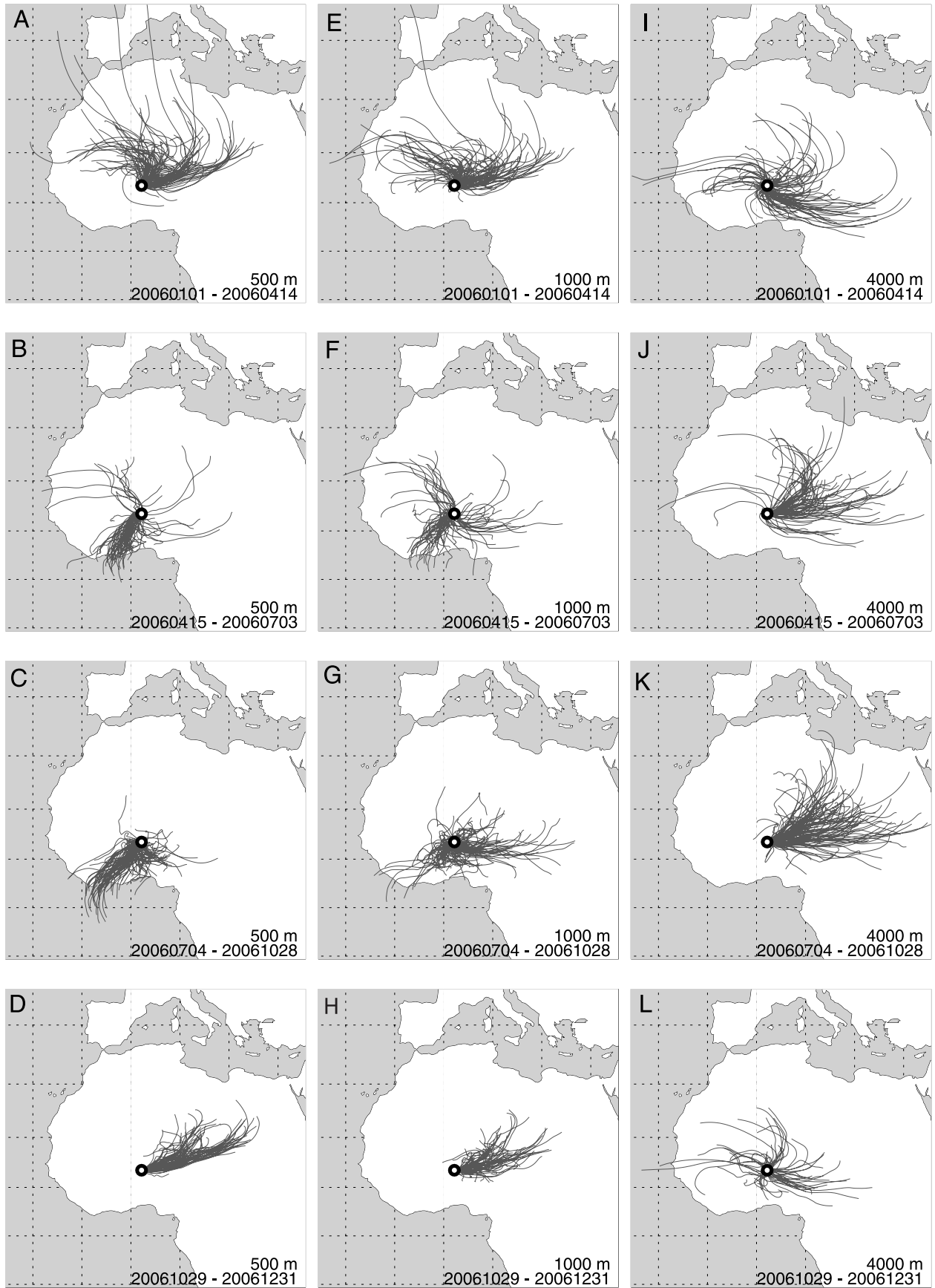


Figure 9

the first occurrence of monsoon air at low levels at Niamey but ending before the northward ITF passage (Figure 3); the first part of the wet season up to 3 July; the second part of the wet season including the rest of its July–September core; and finally the dry season at the end of the year that begins on 29 October as the ITF moves south of Niamey (Figure 3).

[36] During the dry season at the start of the year (Figures 9a, 9e, and 9i), the air at 500 m over Niamey came primarily from the north and east, associated with the climatological Harmattan wind. The preferred source regions of the Bodélé depression centered on 17°N, 17°E [Washington *et al.*, 2006] and the Massif de l’Air (17°N, 7°E) are evident, although trajectories cover a wide range of other locations over the southern Sahara. The very long trajectories that begin in southern Europe occurred during the major dust storm in early March 2006 [Slingo *et al.*, 2006], as is also shown by Milton *et al.* [2008]. The results at 1000 m are very similar, but at 4000 m a large fraction of the trajectories originate to the south and east of Niamey, e.g., over Nigeria. Here, aerosols from biomass burning are injected into the atmosphere and arrive over Niamey at levels much higher than the low-level Harmattan flow. This is in agreement with the analysis of the DABEX data from January 2006 described by Haywood *et al.* [2008], and is further illustrated by the sonde data in the section 4.4.

[37] Figures 9b, 9f, and 9j start with the “false” monsoon onset on 15 April and cover the first part of the wet season. The low-level trajectories arriving from the north occur during late April, before the monsoon flow is fully established. Following the true (and delayed) onset on 5 May, there is a marked change in the direction of the back trajectories at 500 m and to a lesser extent at 1000 m, indicating the arrival of the moist air from the Gulf of Guinea. At 4000 m, the winds are primarily from the east, associated with the development of the African Easterly Jet. Later in the wet season (Figures 9c, 9g, and 9k), the flow at 500 m is almost exclusively from the southwest, while the flow at the two higher levels again shows the effect of the climatological flow from the east.

[38] Figures 9d, 9h, and 9l cover the return of dry season conditions, following the retreat of the monsoon to the south of Niamey on 29 October. At 500 m and 1000 m, the tracks are much more tightly defined in direction than at the start of the year and show that the air arriving in Niamey is influenced by the source regions of the Bodélé and Massif de l’Air. At 4000 m, the trajectories revert to the more variable directions evident in Figure 9i, but again show that some of the air comes from the southeast.

[39] These results are in good agreement with the source regions derived by Schepanski *et al.* [2007] from SEVIRI data for March 2006 to February 2007. Their results clearly show the Bodélé and Massif de l’Air as preferred source regions for Niamey, as well as a broad region of the

southern Sahara to the north of Niamey, consistent with the trajectories shown in Figure 9.

4.4. Atmospheric Structure for Selected Cases

[40] Selected rawinsonde ascents and range-corrected backscatter plots from the micropulse lidar at the AMF airport site are shown in Figures 10 and 11, to illustrate events that are either analyzed in more detail in the following papers, or are typical of conditions over an extended period. With over a year of data, there are many other days that could have been chosen. Those shown here were selected in part because they cover the complete range of aerosol loadings encountered over the year, consistent with the goal in some of the subsequent work of characterizing the aerosol properties and their impact on the radiation budget.

[41] At the beginning of 2006, during the dry season, the atmosphere over Niamey frequently showed multiple layers in the midtroposphere, separated by inversions, with large changes in humidity between the layers. Near the surface, solar heating created a well-mixed layer to 850–900 hPa in the daytime, but the strong diurnal cycle in surface temperature led to the formation of a stable layer near the surface overnight. Figure 10a illustrates these features for the sonde released on 21 January during the DABEX campaign. Osborne *et al.* [2008] present an analysis of the aircraft data from flight B160 on this day. They found a dust aerosol layer extending from the surface (984 hPa) to about 900 hPa, above which was a layer of biomass burning aerosols from about 780 to 600 hPa. The positions of these two aerosol layers are indicated on Figure 10a, which shows that each layer is capped by a small inversion. The layering of the different aerosol types is consistent with the trajectory analysis shown in Figures 9a, 9e, and 9i. The layers are also apparent on the corresponding MPL backscatter plot (Figure 11a), which shows considerable variability in time as the heterogeneous aerosol structures are advected over the site. Figure 11a also shows that backscatter measurements at a single wavelength cannot distinguish between the two aerosol types. The MPL data and those from the Multifilter Rotating Shadowband Radiometer (MFRSR) on this day are analyzed in detail by McFarlane *et al.* [2008] in another paper in this special section.

[42] Another common occurrence during the dry season at the start of the year was the detection of very thin cloud layers at the top of the highest aerosol layer and also at higher levels, where humidities just reached saturation below the inversions. Such layers are evident in the MPL plot (Figure 11a) in the evening, at 7 km (430 hPa) at the time of the sonde, and at about 5 km at the top of the biomass aerosol layer just before midnight.

[43] As the dry season progressed, the increasing surface temperatures shown in Figure 5 led to the development of much deeper near-surface mixed layers in the daytime. On

Figure 10. Skew-T log-p plots of temperatures (black lines) and dew point temperatures (blue lines) for six representative AMF rawinsondes launched from Niamey. The dates and launch times of the sondes are shown above each plot. The two bars on the plot for 21 January represent the approximate vertical extents of the biomass aerosol layer (top bar) and dust aerosol layer (bottom bar) observed by the UK BAe146 research aircraft during DABEX flight B160 [Osborne *et al.*, 2008].

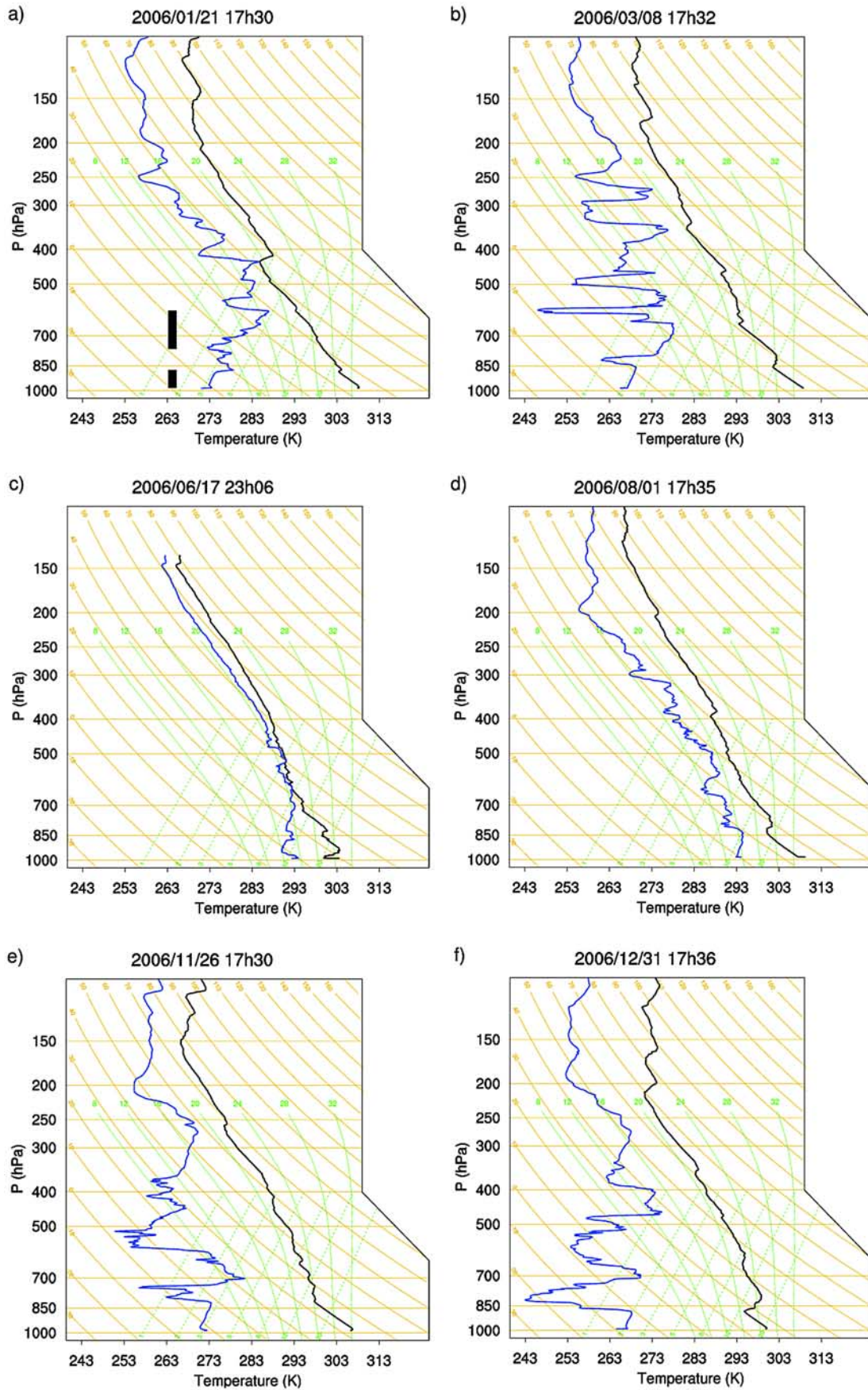


Figure 10

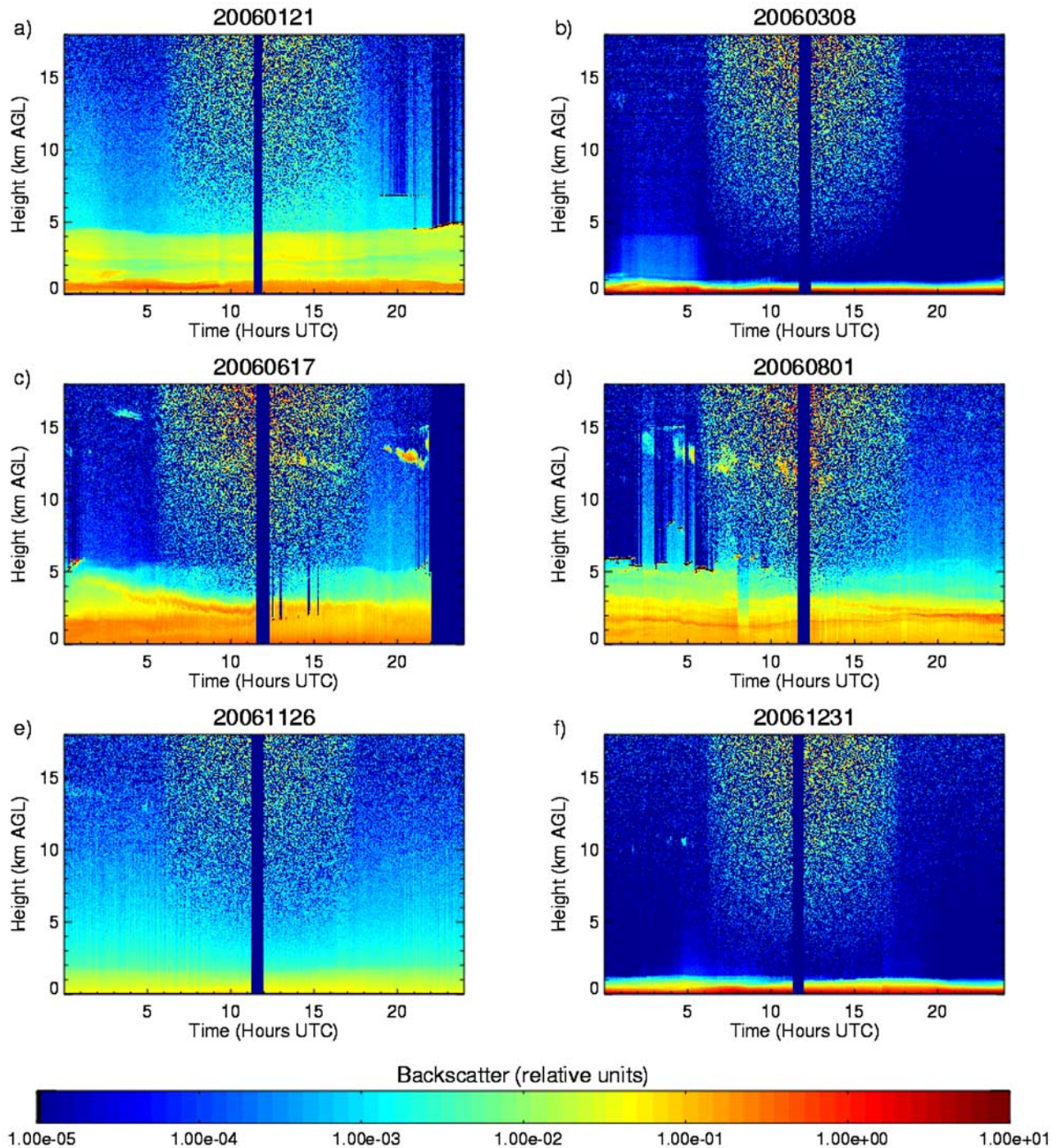


Figure 11. Range-corrected micropulse lidar (MPL) backscatter profiles (in relative units) over 24 h for the same days as the rawinsondes shown in Figure 10. The dates are shown above each plot. The vertical blue bands at about 1200 UTC on each day denote missing data when a shutter operated to prevent direct sunlight from entering the detector optics. The enhanced noise at upper levels during daylight hours is caused by interference from scattered sunlight (note that local time is the same as UTC in Niamey). The bright, diffuse colors at low levels are due to backscatter from aerosols. The red spots show the bases of optically thick clouds, which the Lidar beam cannot penetrate, while the diffuse colored backscatter at upper levels is due to optically thin cirrus.

6 March, for example, the afternoon sonde (not shown here) indicated a well-mixed layer extending uninterrupted from the surface to 600 hPa. The following day, a surge of cold air from the Northern Hemisphere extratropics produced a

major dust storm over much of West Africa [Slingo *et al.*, 2006]. The layer of cold, but well-mixed, air, extending from near the surface up to 860 hPa, can be seen on the sonde ascent for 8 March shown in Figure 10b. The intense

backscatter from the aerosol is readily apparent in Figure 11b. *Slingo et al.* [2006] provide more detail on that striking event.

[44] The dramatic change in atmospheric structure during the wet season is illustrated by Figure 10c, which shows a sonde ascent for just before midnight on 17 June. The atmosphere is far more moist than in Figures 10a and 10b and shows evidence of deep convection reaching the tropopause. On that evening, an intense convective storm passed directly over the site and caused some damage to the instruments and loss of data, as witnessed by the missing data on the right hand side of the MPL plot (Figure 11c). Nevertheless, as the plot clearly shows, the previous day was almost cloud-free, with small amounts of cirrus and thin, low cloud. This is typical of the relatively dry monsoon season in Niamey in 2006: convective events usually lasted for no more than a few hours and were often interspersed with days of suppressed and almost cloud-free conditions. Aerosol, however, appeared to be ubiquitous in the lowest few kilometers, as is evident on Figure 11c. Once again, there is considerable structure in the aerosol, with multiple layers extending to 5 km. Animations of the satellite imagery show dust being lofted by convective downdrafts, often spreading outward in almost circular, expanding features. These are most clearly seen to the north of the main convective regions, as the downdrafts propagate into the desert. At Niamey, it was usually not possible to associate the aerosol structures such as those illustrated by Figure 11c directly with such events, in part because high water vapor loadings obscured the aerosol signals in the satellite imagery.

[45] *Miller and Slingo* [2007] show data from several key AMF instruments [*Miller and Slingo*, 2007, Figure 8] and the sonde ascent [*Miller and Slingo*, 2007, Figure 7] for 9 July, another convective day during the wet season. Comparison of the sonde ascent given by *Miller and Slingo* [2007, Figure 7] with Figure 10c here illustrates the variety of structures associated with convective activity. Their MPL plot also demonstrates that this instrument cannot penetrate thick clouds, information on the cloud vertical structure coming instead from the 95 GHz cloud radar. Although not obvious in the measurements shown by *Miller and Slingo* [2007], many such days show the signatures of 3-D cloud effects in the radiation fields, which complicates the interpretation of the radiometer data at this time of the year.

[46] Figures 10d and 11d show the final examples of atmospheric structure for the wet season (1 August). This was a day with broken high cloud and extensive aerosol, with multiple layers evident on the MPL plot. Thin medium-level cloud is again evident at around 6 km. The sonde temperature profile is less convective than on 17 June and is remarkably similar to that for 8 March (Figure 10b) in the free troposphere. Near the surface is a well-mixed layer which contains most of the dust aerosol. *Taylor et al.* [2007] present an analysis of data from an aircraft flight to the northwest of Niamey on this day, which show that meso-scale atmospheric circulations can be induced in this region by horizontal variations in soil moisture in the underlying surface.

[47] The final two examples of atmospheric structure come from the dry season following the retreat of the ITF southward on 29 October. The first shows the data for

26 November (Figures 10e and 11e), one of only a few days in 2006 with unusually low amounts of aerosol, providing the nearest conditions to “pristine” (i.e., aerosol-free) for testing radiation codes (N. A. Bharmal et al., Simulation of surface and top of atmosphere thermal fluxes and radiances from the RADAGAST experiment, submitted to *Journal of Geophysical Research*, 2008). Only low levels of backscatter from aerosol can be seen on the MPL backscatter plot (Figure 11e). In contrast, at the end of the year a substantial dust storm originated over the Bodélé depression on 27 December, sending daily pulses of dust in a wide arc toward Niamey. By 31 December, the MPL showed a thick dust layer over the site (Figure 11f), although not as extreme as in the March event. Despite the differences in the aerosol loadings, the sondes for these two days are actually very similar (Figures 10e and 10f), with many stable layers in the free troposphere and some nearly well-mixed layers in between. The only obvious difference is that the sonde for 31 December shows a cooler, shallower surface mixed layer beneath a strong capping inversion. This ascent is similar to that for 8 March (Figure 10b), except that the geographical origin of the colder air near the surface was different.

[48] One curious feature seen in the MPL data (but not shown here) is a tendency for a plume of aerosol to appear at low levels in the early hours of the morning; typically around 0300 local time. This appears to be associated with the nocturnal jet, which was observed to peak at that time in other studies during AMMA [*Lothon et al.*, 2008].

5. Summary and Discussion

[49] Observations of meteorological and thermodynamic variables obtained during the RADAGAST experiment in Niamey, Niger, during 2006 are presented in this paper. Apart from a few brief periods, these data provide a continuous record of the substantial changes in conditions that occurred through the annual cycle of dry and wet seasons. The experiment combined surface observations from the U.S. Department of Energy’s Atmospheric Radiation Measurement (ARM) Program Mobile Facility (AMF) in Niamey with SEVIRI and GERB data from the Meteosat-8 operational geostationary satellite.

[50] The observations from the AMF and from many other stations in West Africa in 2006 are contrasted with the long-term climate averages of this region. Compared with the long-term mean, the onset of the wet season was delayed by about a month and rainfall was deficient in Niamey during most of the season. There was an abrupt end to the wet season, as documented by several different parameters. The contrast between humidities in the wet and dry seasons was marked, with surface dew points ranging from well below 0°C throughout most of the dry season to over 20°C at the height of the wet season. The rawinsonde profiles reveal a rich and varied vertical structure in temperatures, humidities and winds. The column water vapor ranged from 3 mm just before the start of the wet season to around 60 mm at its height. This large range provides excellent opportunities for testing radiation codes, although a complicating factor is that aerosols (mainly dust) are almost ubiquitous throughout the year. The dust loadings show large variability, however, so that not only were there several events with substantial amounts of aerosol but

also some extremely clear days, notably toward the end of the year. This variability is exploited in the following papers to quantify the dependence of the radiative fluxes on both the water vapor and dust loadings.

[51] Back trajectories were used to determine the source of the air arriving over Niamey. In the dry season, the low-level Harmattan flow brought dust-laden air from the north and east. Preferential source regions such as the well-known Bodélé depression were clearly identified. At higher levels, air from the southeast carried aerosols from near-equatorial African regions of biomass burning, as found in the DABEX aircraft observations [Osborne *et al.*, 2008]. In the wet season, the low-level southwesterly flow brought monsoon air from the Gulf of Guinea, while at lower midtropospheric levels the climatological easterlies were associated with the African Easterly Jet.

[52] Selected rawinsonde ascents and lidar backscatter plots were shown to illustrate the range of atmospheric vertical structures observed during the year. Multiple layers, often including aerosols and separated by inversions, were common during the dry seasons and on many occasions during the wet season as well. Major dry season dust events, such as those in early March and in late December, were associated with large-scale dynamical forcing from the Northern Hemisphere extratropics. Dust events in the wet season appeared to be associated with gust fronts from local convection and from mesoscale convective systems.

[53] In Part 2 of this overview (Slingo *et al.*, submitted manuscript, 2008), the radiative fluxes at the top of the atmosphere and at the surface are presented and the factors that control these fluxes are examined. Analysis of the divergence of the fluxes across the atmosphere is also included. Subsequent papers in this special section deal with comparisons of the observed thermal radiative fluxes with those simulated by a radiative transfer code [Bharmal *et al.*, 2008]; analysis of the effects of heterogeneities on estimates of radiative divergence, including exploitation of the data from the ancillary AMF site at Banizoumbou [Settle *et al.*, 2008]; retrievals of aerosol properties from spectrally resolved measurements at the AMF airport site [McFarlane *et al.*, 2008; Turner, submitted manuscript, 2008]; observations of cloud vertical structure and of precipitation (P. Kollias *et al.*, Cloud and precipitation observations during the 2006 ARM Mobile Facility deployment in Niamey, Niger, Africa, submitted to *Journal of Geophysical Research*, 2008); and with seasonal variations in the components of the surface energy balance (R. L. Miller *et al.*, Seasonal contrasts in the surface energy balance of the Sahel, submitted to *Journal of Geophysical Research*, 2008).

[54] **Acknowledgments.** This paper is a combined UK-USA contribution to the multinational African Monsoon Multidisciplinary Analysis (AMMA) Project and the Atmospheric Radiation Measurement (ARM) Program of the U.S. Department of Energy. The deployment of the ARM Mobile Facility (AMF) in Niger during 2006 was funded by the Office of Biological and Environment Research, Office of Science, U.S. Department of Energy. Analyses of the AMF and other data were performed at the University of Reading with support by the UK Natural Environment Research Council; at the University of Oklahoma with support by the Office of Science (BER), U.S. Department of Energy, grant DE-FG02-05ER64062; at the University of Wisconsin-Madison with support by the Office of Science (BER), U.S. Department of Energy, grant DE-FG02-06ER64167; and at the Pacific Northwest National Laboratory with support by the Office of Science (BER), U.S. Department of Energy under contract

DE-AC06-76RL01830. M. Miller is funded by the Environmental Sciences Department at Rutgers University and the Department of Energy through Brookhaven Science Associates, LLC, under contract DE-AC02-98CH10866. The Pacific Northwest National Laboratory is operated by Battelle for the U.S. Department of Energy. Long-term meteorological data were provided by the National Weather Services of Mali, Burkina Faso, Ghana, Benin, Niger, Nigeria, and Chad. The AMMA rain gauge data used in section 3.1 were obtained from the official AMMA data archive. The trajectory calculations were performed by Rick Wagener of the ARM External Data Center at Brookhaven National Laboratory. We thank EUMETSAT for providing limited area subsets of the SEVIRI radiances in near-real time. It is also a pleasure to reiterate the debt owed to the individuals acknowledged by Miller and Slingo [2007] for their contributions to making the deployment of the AMF in Niamey a success. The quantity and quality of the data obtained from the AMF would not have been possible without their professionalism and dedication. The constructive suggestions of two formal reviewers sharpened the manuscript.

References

- Ackerman, T. P., D. M. Flynn, and R. T. Marchand (2003), Quantifying the magnitude of anomalous solar absorption, *J. Geophys. Res.*, *108*(D9), 4273, doi:10.1029/2002JD002674.
- Bell, M. A., and P. J. Lamb (2006), Integration of weather system variability to multidecadal regional climate change: The West African Sudan-Sahel zone, 1951–98, *J. Clim.*, *19*, 5343–5365, doi:10.1175/JCLI4020.1.
- Draxler, R. R. (2006), The use of global and mesoscale meteorological model data to predict the transport and dispersion of tracer plumes over Washington, D.C., *Weather Forecast.*, *21*, 383–394, doi:10.1175/WAF926.1.
- Eldridge, R. H. (1957), A synoptic study of West African disturbance lines, *Q. J. R. Meteorol. Soc.*, *83*, 303–314, doi:10.1002/qj.49708335704.
- Harries, J. E., *et al.* (2005), The Geostationary Earth Radiation Budget (GERB) project, *Bull. Am. Meteorol. Soc.*, *86*, 945–960, doi:10.1175/BAMS-86-7-945.
- Hastenrath, S. (1991), *Climate Dynamics of the Tropics*, Kluwer Acad., Dordrecht, Netherlands.
- Hastenrath, S., and P. Lamb (1977), Some aspects of circulation and climate over the eastern equatorial Atlantic, *Mon. Weather Rev.*, *105*, 1019–1023, doi:10.1175/1520-0493(1977)105<1019:SAOCAC>2.0.CO;2.
- Haywood, J., P. Francis, S. Osborne, M. Glew, N. Loeb, E. Highwood, D. Tanré, G. Myhre, P. Formenti, and E. Hirst (2003), Radiative properties and direct radiative effect of Saharan dust measured by the C-130 aircraft during SHADE: 1. Solar spectrum, *J. Geophys. Res.*, *108*(D18), 8577, doi:10.1029/2002JD002687.
- Haywood, J. M., *et al.* (2008), Overview of the Dust and Biomass-burning Experiment and African Monsoon Multidisciplinary Analysis Special Observing Period-0, *J. Geophys. Res.*, doi:10.1029/2008JD010077, in press.
- Ilesanmi, O. O. (1971), An empirical formulation of an ITD rainfall model for the tropics: A case study for Nigeria, *J. Appl. Meteorol.*, *10*, 882–891, doi:10.1175/1520-0450(1971)010<0882:AEFOAI>2.0.CO;2.
- Källberg, P., P. Berrisford, B. Hoskins, A. Simmons, S. Uppala, S. Lamy-Thépaut, and R. Hine (2005), ERA-40 atlas, *ERA-40 Proj. Rep. Ser.*, *19*, Eur. Cent. for Med.-Range Weather Forecasts, Reading, U. K. (Available at <http://www.ecmwf.int/publications>)
- Lamb, P. J. (1978), Large-scale tropical Atlantic surface circulation patterns associated with Subsaharan weather anomalies, *Tellus*, *30*, 240–251.
- Lélé, M. I., (2007), Variability of Intertropical Front (ITF) and rainfall over West African Soudano-Sahel zone, M. S. thesis, 92 pp., Sch. of Meteorol., Univ. of Okla., Norman.
- Lothon, M., F. Saïd, F. Lohou, and B. Campistron (2008), Observation of the diurnal cycle in the low troposphere of West Africa, *Mon. Weather Rev.*, *136*, 3477–3500.
- McFarlane, S. A., E. I. Kassianov, J. C. Barnard, C. Flynn, and T. Ackerman (2008), Surface shortwave aerosol radiative forcing during the ARM Mobile Facility deployment in Niamey, Niger, *J. Geophys. Res.*, doi:10.1029/2008JD010491, in press.
- Miller, M. A., and A. Slingo (2007), The ARM Mobile Facility and its first international deployment: Measuring radiative flux divergence in West Africa, *Bull. Am. Meteorol. Soc.*, *88*, 1229–1244, doi:10.1175/BAMS-88-8-1229.
- Milton, S. F., G. Greed, M. E. Brooks, J. Haywood, B. Johnson, R. P. Allan, A. Slingo, and W. M. F. Grey (2008), Modeled and observed atmospheric radiation balance during the West African dry season: Role of mineral dust, biomass burning aerosol, and surface albedo, *J. Geophys. Res.*, *113*, D00C02, doi:10.1029/2007JD009741.
- Nicholson, S. E., and J. P. Grist (2003), The seasonal evolution of the atmospheric circulation over West Africa and equatorial Africa, *J. Clim.*, *16*, 1013–1030, doi:10.1175/1520-0442(2003)016<1013:TSEOTA>2.0.CO;2.

- Osborne, S. R., B. T. Johnson, J. M. Haywood, A. J. Baran, M. A. J. Harrison, and C. L. McConnell (2008), Physical and optical properties of mineral dust aerosol during the Dust and Biomass-burning Experiment, *J. Geophys. Res.*, *113*, D00C03, doi:10.1029/2007JD009551.
- Ramanathan, V., et al. (2001), Indian ocean experiment: An integrated analysis of the climate forcing and effects of the great Indo-Asian haze, *J. Geophys. Res.*, *106*, 28,371–28,398, doi:10.1029/2001JD900133.
- Redelsperger, J.-L., C. D. Thorncroft, A. Diedhiou, T. Lebel, D. J. Parker, and J. Polcher (2006), African Monsoon Multidisciplinary Analysis. An international research project and field campaign, *Bull. Am. Meteorol. Soc.*, *87*, 1739–1746, doi:10.1175/BAMS-87-12-1739.
- Schepanski, K., I. Tegen, B. Laurent, B. Heinhold, and A. Macke (2007), A new Saharan dust source activation frequency map derived from MSG-SEVIRI IR-channels, *Geophys. Res. Lett.*, *34*, L18803, doi:10.1029/2007GL030168.
- Schmetz, J., P. Pili, S. Tjemkes, D. Just, J. Kerkman, S. Rota, and A. Ratier (2002), An introduction to Meteosat Second Generation (MSG), *Bull. Am. Meteorol. Soc.*, *83*, 977–992, doi:10.1175/1520-0477(2002)083<0977:AITMSG>2.3.CO;2.
- Segele, Z. T., and P. J. Lamb (2005), Characterization and variability of Kiremt rainy season over Ethiopia, *Meteorol. Atmos. Phys.*, *89*, 153–180, doi:10.1007/s00703-005-0127-x.
- Settle, J. J., N. A. Bharmal, G. J. Robinson, and A. Slingo (2008), Sampling uncertainties in surface radiation budget calculations in RADAGAST, *J. Geophys. Res.*, doi:10.1029/2008JD010509, in press.
- Slingo, A., et al. (2006), Observations of the impact of a major Saharan dust storm on the atmospheric radiation balance, *Geophys. Res. Lett.*, *33*, L24817, doi:10.1029/2006GL027869.
- Taylor, C. M., D. J. Parker, and P. P. Harris (2007), An observational case study of mesoscale atmospheric circulations induced by soil moisture, *Geophys. Res. Lett.*, *34*, L15801, doi:10.1029/2007GL030572.
- Turner, D. D., S. A. Clough, J. C. Liljegren, E. E. Clothiaux, K. E. Cady-Pereira, and K. L. Gaustad (2007), Retrieving liquid water path and precipitable water vapor from the Atmospheric Radiation Measurement (ARM) microwave radiometers, *IEEE Trans. Geosci. Remote Sens.*, *45*, 3680–3690, doi:10.1109/TGRS.2007.903703.
- Washington, R., M. C. Todd, S. Engelstaedter, S. Mbainayel, and F. Mitchell (2006), Dust and the low-level circulation over the Bodélé Depression, Chad: Observations from BoDEx 2005, *J. Geophys. Res.*, *111*, D03201, doi:10.1029/2005JD006502.
- R. P. Allan, N. A. Bharmal, G. J. Robinson, J. J. Settle, A. Slingo, and H. E. White, Environmental Systems Science Centre, University of Reading, Reading RG6 6AL, UK. (as@mail.nerc-essc.ac.uk)
- J. Barnard, C. Flynn, E. Kassianov, and S. McFarlane, Pacific Northwest National Laboratory, Richland, WA 99352, USA.
- P. J. Lamb and M. I. Lélé, CIMMS, University of Oklahoma, Norman, OK 73072, USA.
- M. Miller, Environmental Sciences Department, Rutgers University, 14 College Farm Road, New Brunswick, NJ 08901-8551, USA.
- D. D. Turner, Space Science and Engineering Center, University of Wisconsin-Madison, Madison, WI 53706, USA.